Since January 2020 Elsevier has created a COVID-19 resource centre with free information in English and Mandarin on the novel coronavirus COVID-19. The COVID-19 resource centre is hosted on Elsevier Connect, the company's public news and information website.

Elsevier hereby grants permission to make all its COVID-19-related research that is available on the COVID-19 resource centre - including this research content - immediately available in PubMed Central and other publicly funded repositories, such as the WHO COVID database with rights for unrestricted research re-use and analyses in any form or by any means with acknowledgement of the original source. These permissions are granted for free by Elsevier for as long as the COVID-19 resource centre remains active.

Separation and Purification Technology 279 (2021) 119625

Contents lists available at ScienceDirect

Separation and Purification Technology

journal homepage: www.elsevier.com/locate/seppur

A highly efficient nanofibrous air filter membrane fabricated using electrospun amphiphilic PVDF-*g*-POEM double comb copolymer

Juyoung Moon [a,1], Tan Tan Bui [b,1], Soyoung Jang [c], Seungyoung Ji [c], Jung Tae Park [a,*], Myung-Gil Kim [b,*]

[a] Department of Chemical Engineering, Konkuk University, 120 Neungdong-ro, Gwangjin-gu, Seoul 05029, Republic of Korea
[b] School of Advanced Materials Science & Engineering, Sungkyunkwan University, 2066 Seobu-ro, Jangan-gu, Suwon 16419, Republic of Korea
[c] LEMON Co., 1105-65, Sanho-daero, Sandong-eup, Gumi 39170, Republic of Korea

ARTICLE INFO

Keywords:
COVID-19
Air filter
Electrospinning
Nanofibers
Atomic transfer radical polymerization (ATRP)
Double comb copolymer

ABSTRACT

Current global emergencies, such as the COVID-19 pandemic and particulate matter (PM) pollution, require urgent protective measures. Nanofibrous air filter membranes that can capture $PM_{0.3}$ and simultaneously help in preventing the spread of COVID-19 are essential. Therefore, a highly efficient nanofibrous air filter membrane based on amphiphilic poly(vinylidene fluoride)-*graft*-poly(oxyethylene methacrylate) (PVDF-*g*-POEM) double comb copolymer was fabricated using atomic transfer radical polymerization (ATRP) and electrospinning. Fourier transform infrared spectroscopy, X-ray diffraction, proton nuclear magnetic resonance, transmission electron microscopy, differential scanning calorimetry, and thermogravimetric analysis were employed to successfully characterize the molecular structure of the fabricated amphiphilic PVDF-*g*-POEM double comb copolymer. The nanofibrous air filter membrane based on amphiphilic PVDF-*g*-POEM double comb copolymer achieved a low air resistance of 4.69 mm H_2O and a high filtration efficiency of 93.56 % due to enhanced chemical and physical adsorption properties.

1. Introduction

The COVID-19 pandemic has become an extremely urgent global concern owing to the serious threat of an exponential increase in the number of infected patients and confirmed deaths, which are already at more than 173 million and 3.7 million, respectively, according to the WHO as of June 8, 2021. Even though COVID-19 vaccines are being successfully distributed in several countries, critical issues such as long-term vaccine preservation for worldwide distribution and the possibility of short supply remain. Therefore, temporary prevention methods, such as handwashing and social distancing are important.

Among these methods, wearing face masks is a fundamental and extremely safe option that can enhance the effectivity against virus transmission up to 79 %.[1,2] In general, face mask and air filtration industries have been developed to deal with air pollution, especially with respect to particulate matter ($PM_{2.5}$, $PM_{1.0}$, $PM_{0.3}$); PM is known to have a considerable impact on the human respiratory system, and can result in congestive heart failure or lung cancer. [3–6] Among these fine dusts, $PM_{0.3}$ is referred to as the most penetrating particle size, implying its inability to be effectively filtered out by conventional mechanical filter membranes. [7,8] Therefore, devices that can effectively filter such PM are rare. Long-lived hazardous microdusts and the on-going COVID-19 pandemic both threaten the human environment and inhibit the improvement of public health. Disposable face masks with physical filtering mechanisms have been frequently used over the last year. [9,10] Numerous studies have investigated the development of a suitable air filtration system that can impede the absorption of airborne PM through inhalation and preclude the spread of COVID-19-containing droplets. [11,12] Currently, fibrous-filter-based N95 masks are the state-of-the-art owing to their physical sieving ability; these are mostly fabricated using the melt-blown (MB) process. [7,13] However, these melt-blown mask filters are known to suffer from issues, such as poor reliability for long term usage and filtration performance degradation due to charge loss under exposure in organic solvent, such as ethanol, isopropanol. [14,15]

Electrospun nanofibers have been considered as the most feasible

* Corresponding authors.
E-mail addresses: jtpark25@konkuk.ac.kr (J.T. Park), myunggil@skku.edu (M.-G. Kim).
[1] J. Moon, T. T. Bui contributed equally to this work.

https://doi.org/10.1016/j.seppur.2021.119625
Received 15 June 2021; Received in revised form 26 August 2021; Accepted 29 August 2021
Available online 11 September 2021
1383-5866/© 2021 Elsevier B.V. All rights reserved.

alternative owing to the simplicity of processing and compatibility with several polymers; fibers with a wide range diameter can be produced, which contributes to the diversity of fabrication systems. [16–18] Electrospinning is a novel method that facilitates the construction of ultrathin nanofibrous-web membranes with a significantly high air permeability and relatively low pressure drop, owing to the well-known slip effect that occurs when the fiber diameters are similar to the size of air molecules. [19–22] However, the simple nanofiber-based filters still exhibit a poorer initial air filtration performance to the performance of electret based MB filter. Further improvement in air filtration performance of NF membrane is urgent to replace the commercial MB filter.

Known as one of the living radical polymerizations, atomic transfer radical polymerization (ATRP) is a widely used method to prepare block copolymers from polymeric initiators, polymer chains with ordered space, and pendant chemical groups with radically transferable halogen atoms. [23] Poly(vinylidene fluoride) (PVDF) based copolymer *via* ATRP is typically used as a binder, separator, electrolyte and membrane in green technology devices, due to its decent chemical and thermal stability and piezoelectric response. [24–27] Also, nanofibrous air filter membrane based on highly polar β phase of PVDF is expected to improve polarizability and net dipole moment, which eventually would lead to increase filtration efficiency. [28] Nevertheless, the conventional electrospun PVDF nanofibers were found to show inhomogeneously beaded structure at low concentration with insufficient viscosity and instability of polymer jet. [29] Further modifications were implemented to improve the filtration efficiency, such as adding surfactant to remove beads on fibers and simultaneously decrease nanofiber diameter [30] or fabricating tree-like structure to enhance the particles capturing ability. [31] Meanwhile, the use of amphiphilic double comb copolymer PVDF-*g*-POEM in green technology devices is advantageous due to the low cost, the easiness to synthesize and *etc.*, compared to that of block or graft typed copolymer such as PVDF-TrFE. Recently, we have successfully prepared a double comb copolymer (PVDC-*g*-POEM), directly grafted with a hydrophilic POEM by introducing ATRP from secondary chlorines on the main chain backbone *via* ATRP. [32–34] Furthermore, amphiphilic co-polymers can take advantage of both physical and chemical aspects. As a chemical aspect, because it has both a hydrophobic and a hydrophilic nature can filter the dust with the respective characteristic. In addition to the physical advantage due to the thin filter diameter caused influence with the slip effect region. However, PVDF-based double comb copolymer are not economically feasible for low-cost air filtration therefore, alternative novel materials have been developed.

In this study, ATRP was employed to synthesize an amphiphilic PVDF-*g*-POEM double comb copolymer with enhanced chemical and physical adsorption properties. The fluorine atom in hydrophobic PVDF and oxygen atoms in the hydrophilic POEM would allow for improved electronegativity and enhanced electrostatic attraction, respectively. The small diameter of the nanofibrous air filter membrane based on amphiphilic PVDF-*g*-POEM double comb copolymer, which is similar to the mean free path of air molecules (65.3 nm), enables high air-filtration efficiency and quality factor because of the slip-flow effect. In addition, reducing the drag forces on the surface of the air filter membrane based on amphiphilic PVDF-g-POEM double comb copolymer in the transition regime of airflow could allow lowing the air resistance.

2. Experimental

2.1. Materials

Commercial PVDF (Solef® 6010) was sourced from Solvay Specialty Polymers (Bollate, Italy). POEM ($M_w = 500$), copper(I) chloride (CuCl), dimethylacetamide (DMAc) and methyl ethyl ketone (MEK) were purchased from Sigma-Aldrich. N-methyl-2-pyrrolidone (NMP greater than 99.5) was obtained from Duksan and 4,40-dimethyl-2,20-dipyridyl (DMDP) was purchased from Thermo Fisher Scientific.

2.2. Synthesis of amphiphilic PVDF-g-POEM double comb copolymer

PVDF (5 g) was dissolved in 50 mL of NMP and stirred overnight. Subsequently, 50 mL of POEM, 0.04 g of CuCl, and 0.23 g of DMDP were consecutively added to the solution, which was purged with N_2 gas for 1 h 40 min. After bubbling with N_2, the polymerization reaction was conducted at 90 °C for 24 h. The obtained copolymer was washed with methanol several times to remove impurities such as CuCl catalyst. The double comb copolymer solution was completely solidified *via* drying in a vacuum oven at 50 °C for 12 h.

2.3. Preparation of doublc comb copolymer solution for nanofibrous air filter membrane

The synthesized amphiphilic PVDF-*g*-POEM double comb copolymers were separately dissolved in a mixed solvent (DMAc:MEK = 5:5) to prepare solutions consisting of 10 wt% of PVDF-*g*-POEM. Then, the double comb copolymer solutions were stirred overnight at 58 °C for 12 h. For comparison, polymer solution based on hydrophobic PVDF as a control group were also tested in parallel.

2.4. Fabrication of nanofibrous air filter membrane

The nanofibrous air filter membrane based on amphiphilic PVDF-*g*-POEM double comb copolymer were fabricated using an electrospinning machine installed with an indoor-box high electric field generator and a grounded collector (NanoNC Co. Ltd., South Korea). The double comb copolymer solutions were first drawn into a syringe directly connected to multi-nozzle setup with one or five metallic spinneret tip (25G) for desired polymer mass area loading. The electrospinning experiment was carefully conducted at feed rate of 1 mL/h and charged at a high DC voltage of 28 kV, which allowed the double comb copolymer jets to emerge from the tip and gather on a collector that was 16-cm away. The nanofibers were directly electrospun on a PET membrane substrate for the air-filtration-efficiency experiments. The entire electrospinning process was implemented at 25 °C with humidity level of around 20 %. A detailed description of the experimental procedure is presented in Scheme 1.

2.5. Characterization

Fourier transform infrared spectroscopy (FT-IR) was employed to analyze the functional groups of amphiphilic PVDF-*g*-POEM double comb copolymer using the Spectrum Two (PerkinElmer) instrument. Differential scanning calorimetry (DSC) measurements were recorded on DSC 200 F3 Maia (Netzsch). ^{1}H nuclear magnetic resonance (NMR) analysis in deuterated DMF was conducted to probe the molecular structure and calculate the composition of POEM using AVANCE 600 (Bruker). The thermal stability of the polymers was examined using a Discovery thermogravimetric analyzer (TA Instruments). The experiment was carried out under an N_2 atmosphere with the temperature ranging from room temperature to 700 °C at a rate of 10 °C/min. The degree of crystallinity of the polymers was investigated by X-ray diffraction (XRD) using a Smartlab (Rigaku) instrument with Cu K_a radiation, a wavelength of 0.154 nm, a scan range of 2θ = 10-40°, and a scan step of $\Delta 2\theta = 0.5°/s$. Nanofibrous air filter membrane prepared using the amphiphilic PVDF-*g*-POEM double comb copolymer and dissolved in DMF were examined by transmission electron microscopy (TEM, JEM-2100). The hydrophilicity of the membrane surface was measured using contact angles using a DSA100 system (Kruss). Field-emission scanning electron microscopy (FE-SEM, JSM-6700F) was employed to observe the morphology of the electrospun nanofibrous air filter membrane based on amphiphilic PVDF-*g*-POEM double comb copolymer charged by Au conductive coating. The image J software was utilized to measure the diameter of nanofibers, with the average diameter being precisely determined within 50 counts. The air filtration

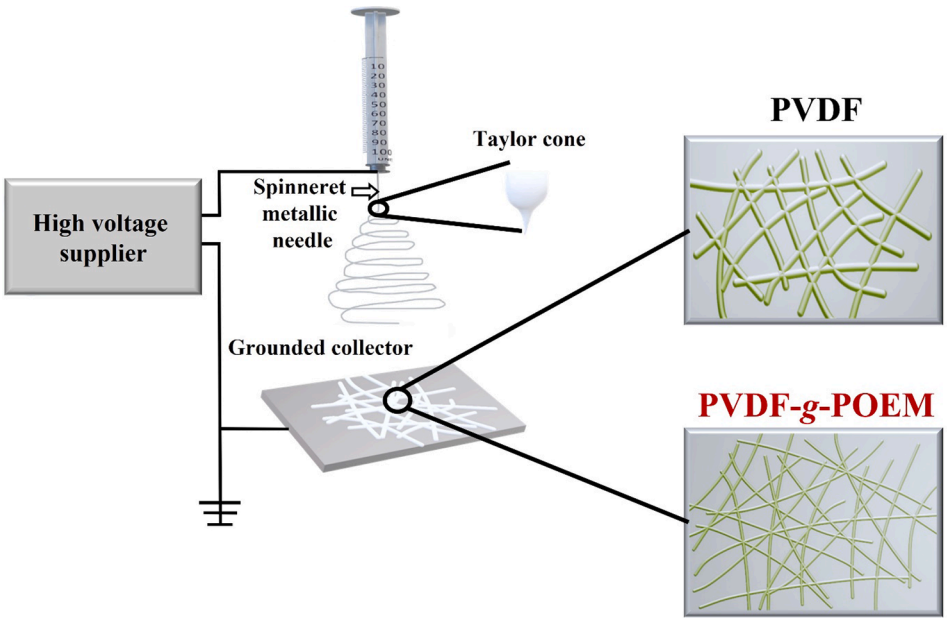

Scheme 1. The illustration of electrospinning for nanofibrous air filter membrane based on hydrophobic PVDF and amphiphilic PVDF-*g*-POEM double comb copolymer.

efficiency was investigated using the TSI-8130 system with an air flow of 5.3 cm/s and NaCl aerogel particles (≤0.3 μm) as simulated PM for determining the filtration efficiency (%) and relative pressure drop (mmH_2O). The overall performance of the filter membranes was estimated using a quality factor parameter defined as follows:

$$QF = -ln(1-\eta)/\Delta P \quad (1)$$

where η and ΔP represent the air filtration efficiency and pressure drop, respectively. The filter test data were averaged for 3 samples.

3. Results and discussion

3.1. Characterization of amphiphilic PVDF-g-POEM double comb copolymer

Scheme 2 illustrates the synthesis reaction of amphiphilic PVDF-*g*-POEM double comb copolymer *via* ATRP. Initiated by the pendant fluorine atoms, hydrophilic POEM side chains were grafted from the hydrophobic PVDF backbone through ATRP. Amphiphilic double comb copolymer (PVDF-*g*-POEM) has interweaved into the hydrophilic regions of PVDF main chains by molecularly self-assembling to the nanophase domains of POEM side chains, which have led to effective control of the chemical and physical adsorption properties.

The FT-IR spectra of hydrophobic PVDF and amphiphilic PVDF-*g*-POEM double comb copolymer are shown in Fig. 1**a**. Upon the polymerization from hydrophobic PVDF, three absorption bands at 2872.2, 1727 and 1100.2 cm^{-1} appeared, attributed to the CH_3 (methyl), C = O (carbonyl), and C-O-C (ester) stretches from POEM, respectively. [32] These FT-IR spectroscopic results demonstrate the successful polymerization of hydrophilic POEM *via* ATRP from the fluorine atoms on the PVDF. The structural changes of hydrophobic PVDF upon polymerization were investigated using XRD analysis, as shown in Fig. 1**b**. Value of *d-spacing* was calculated from the peak maximum using Bragg's law of

$$n\lambda = 2dsin\theta \quad (2)$$

where n is the positive integer, λ is the wavelength (1.5406 Å), d is the inter-planar distance, and θ is the angle from the crystal plane. [35] It should be noted that there was no high crystalline diffraction peak corresponding to the CuCl in the amphiphilic double comb copolymer PVDF-*g*-POEM sample. This indicates that the CuCl catalyst has been removed sufficiently *via* the washing step. The maximum peak position shifted to a higher 2 θ value (from 20° to 20.2°) with the introduction of the POEM side chain, which has followingly resulted to a decrease of the *d-spacing* (from 5.2 Å to 5.0 Å) of the amphiphilic PVDF-*g*-POEM double comb copolymer. These results indicated that the POEM side chain in amphiphilic PVDF-*g*-POEM double comb copolymer has led to the chain contraction in the synthesized polymer matrix and to further control chemical and physical properties. Fig. 1**c** shows the result of the phase composition of amphiphilic PVDF-*g*-POEM double comb copolymer confirmed by FT-IR spectra analysis. And, the corresponding ratio of β phase which is related to polarizability and net dipole moment of amphiphilic PVDF-*g*-POEM double comb copolymer is presented in

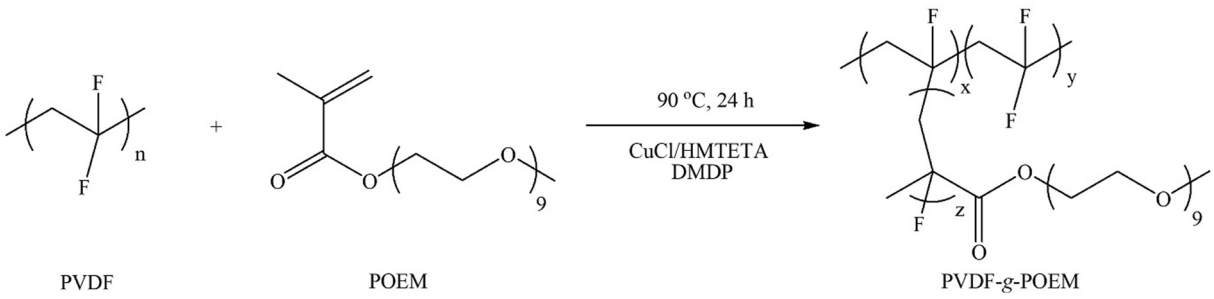

Scheme 2. Atomic transfer radical polymerization of the amphiphilic PVDF-*g*-POEM double comb copolymer.

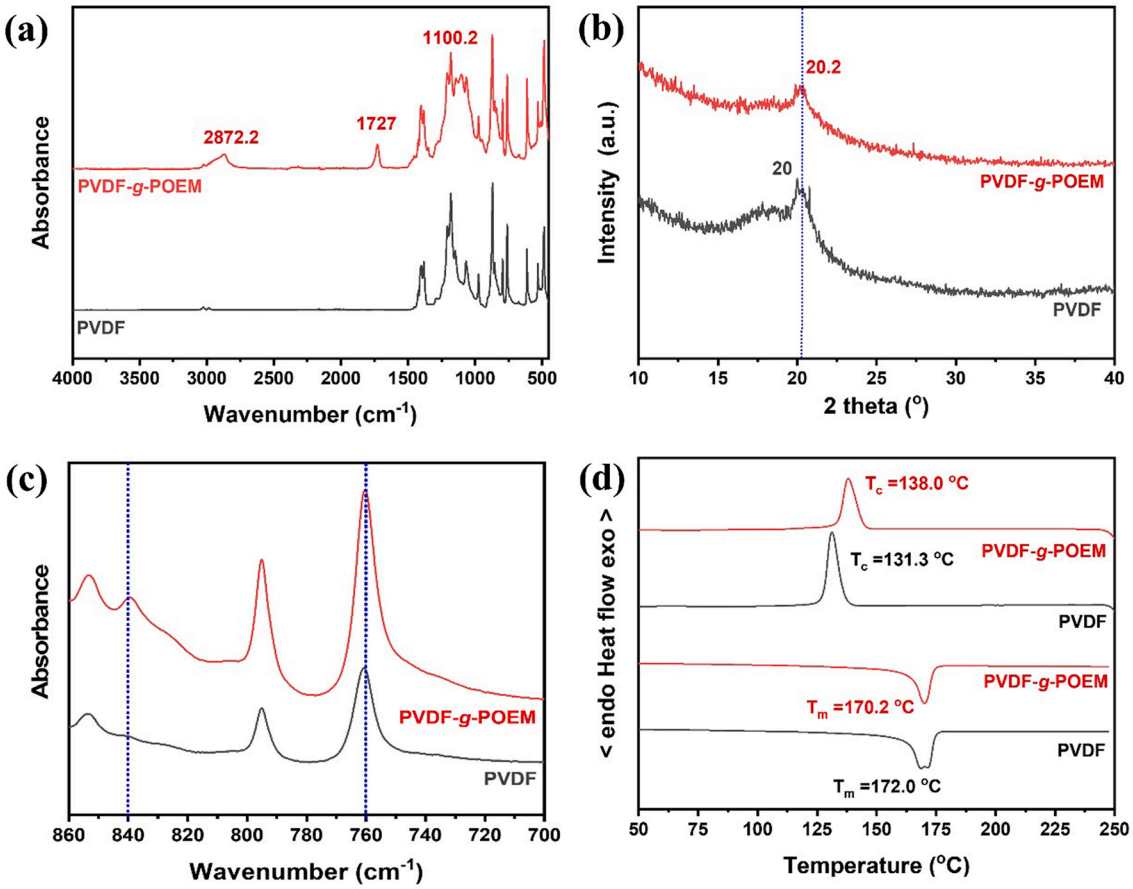

Fig. 1. (a) FT-IR spectra in the range of 4000 to 400 cm^{-1}, (b) XRD, (c) FT-IR spectra in the range of 860 to 700 cm^{-1} and (d) DSC of hydrophobic PVDF and amphiphilic PVDF-*g*-POEM double comb copolymer.

Table 1
β phase content, T_m, T_c and χc of the hydrophobic PVDF and amphiphilic PVDF-*g*-POEM double comb copolymer.[a,b,c]

Polymer	β Phase (%)	T_m (°C)	T_c (°C)	χ_c (%)
PVDF	23.7	172.0	131.3	42.1
PVDF-*g*-POEM	30.3	170.2	138.0	39.2

[a] T_m is melting temperature.
[b] T_c is crystalline temperature.
[c] χ_c is crystallinity.

Table 1. The β phase composition of amphiphilic PVDF-*g*-POEM double comb copolymer was calculated using the following equation

$$F(\beta) = X_\beta/(X_\alpha + X_\beta) = A_\beta/[(\kappa_\beta/\kappa_\alpha)A_\alpha + A_\beta] \quad (3)$$

where F(β) is the ratio of β phase, A_α and A_β are the absorbances at 766 and 840 cm^{-1}, corresponding to the α and β phases in the material, κ_α and κ_β represent the absorption coefficients at the respective wavenumbers, and X_α and X_β represent the degree of crystallinity of each phase. The values of κ_α and κ_β are 6.1×10^4 and 7.7×10^4 cm^2/mol, respectively. [36] The ratio of β phase of amphiphilic PVDF-*g*-POEM double comb copolymer was determined to be 30.3 %, which is approximately 1.3-fold higher than that of the hydrophobic PVDF. These results indicated that the hydrophilic POEM side chain played a significant role as a molecular directing agent to control the phase of amphiphilic PVDF-*g*-POEM double comb copolymer. DSC analyses of the amphiphilic PVDF-*g*-POEM double comb copolymer was performed to determine the melting temperature (T_m), crystalline temperature (T_c) and crystallinity (χ_c), as shown in Fig. 1**d** and Table 1. The crystallinity (χ_c) of amphiphilic PVDF-*g*-POEM double comb copolymer were quantified using the following equation

$$\chi_{c,PVDF-g-POEM}(\%) = \Delta H_{m,PVDF-g-POEM}/\Delta H^{\circ}_{m,PVDF} \cdot 100\% \quad (4)$$

$$\chi_{c,PVDF}(\%) = \Delta H_{m,PVDF}/\Delta H^{\circ}_{m,PVDF} \cdot 100\% \quad (5)$$

where $\Delta H_{m,\ PVDF\text{-}g\text{-}POEM}$ is the melting enthalpy per gram of PVDF-*g*-POEM obtained from the integrated area under the melting peak in the DSC, $\Delta H_{m,\ PVDF}$ is the melting enthalpy per gram of PVDF present in the PVDF-*g*-POEM, $\Delta H_m^{o}{}_{,\ PVDF}$ is the heat of melting per gram of 100% crystalline PVDF, which is taken to be 104.6 J/g. [37] Upon the polymerization of POEM on PVDF, the T_m of PVDF (172.0 °C) shifted to a lower temperature (170.2 °C) while the T_c of PVDF has increased by 6.7 °C to reach 138.0 °C. These observations indicated that the chain mobility in the amphiphilic PVDF-g-POEM double comb copolymer being increased through the transient interaction of segmental chains. It should be noted that the bimodal endothermic peak of hydrophobic PVDF is presumably due to the different head-head and tail–tail isomerism. [38] Furthermore, the $\chi_{c,\ PVDF\text{-}g\text{-}POEM}$ (39.2 %) value was lower than those of $\chi_{c,\ PVDF}$ (42.1 %). These results can be explained by the fact that the crosslinked structure within the PVDF-g-POEM matrix, which could effectively suppress the crystallization process.

To characterize the morphology of amphiphilic PVDF-*g*-POEM double comb copolymer, TEM analysis was carried out (Fig. 2). As shown in Fig. 2**a**, randomly separated nanosized high aspect ratio morphology with black color was shown in the hydrophobic PVDF. Meanwhile, in Fig. 2**b a** clear contrast between the two domains of PVDF and POEM of amphiphilic PVDF-*g*-POEM double comb copolymer was found with the large difference of electron densities. The difference in electron densities

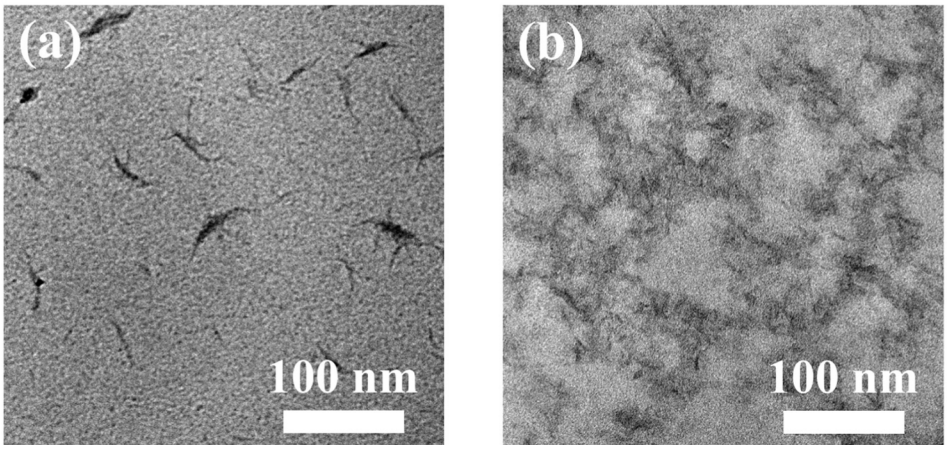

Fig. 2. TEM images of (a) hydrophobic PVDC and (b) amphiphilic PVDF-*g*-POEM double comb copolymer.

between PVDF and POEM of amphiphilic PVDF-*g*-POEM double comb copolymer was large enough to allow distinguishable image contrast between the two regions. Dark regions indicate the hydrophobic PVDF main chains while gray regions indicate the hydrophilic POEM side chains. Also, these observations indicate that the amphiphilic PVDF-*g*-POEM double comb copolymer have molecularly self-assembled into continuous nanophase domains of POEM side chains that is interweaved with hydrophobic domains of PVDF main chains.

The molecular structures of amphiphilic PVDF-*g*-POEM double comb copolymer were elucidated using ^{1}H NMR, as shown in Fig. 3**a**; the solvent peaks are labelled as S_n. The signature peaks of PVDF and POEM are assigned insert molecular structure. The NMR peaks of head-to-head and head-to-tail isomerism of PVDF are denoted by a and a', respectively. The ratio of PVDF and POEM was calculated using the following equations:

$$\varphi_{m(POEM)} == [1/37(I_b + I_c + I_e)]/\left[1/37(I_b + I_c + I_e) + {}^{1}\!/_{2}(I_{a'} + I_a)\right] \quad (6)$$

$$\varphi_{w(POEM)} = [\varphi_{m(POEM)} \cdot M_{(POEM)}]/[\varphi_{m(POEM)} \cdot M_{(POEM)} + \{1 - \varphi_{m(POEM)}\} \cdot M_{(PVDF)}] \quad (7)$$

where $\varphi_{m\ (POEM)}$ and $\varphi_{w\ (POEM)}$ represent the molar and weight ratios of POEM, respectively, I_x is the integral area of the corresponding peak, and M_x represents the molecular weight of each molecule. [39] The two peaks at 3.0 and 2.4 ppm are attributed to the head-to-tail and head-to-head bonding arrangements of PVDF units, respectively. The peaks at 4.1, 3.6, 3.3 and 1.0 ppm are attributed to the H atoms connected to POEM groups in amphiphilic PVDF-*g*-POEM double comb copolymer. As a result, it was found that the amphiphilic PVDF-*g*-POEM double comb copolymer has a composition of 80:20 wt%, respectively. The thermal

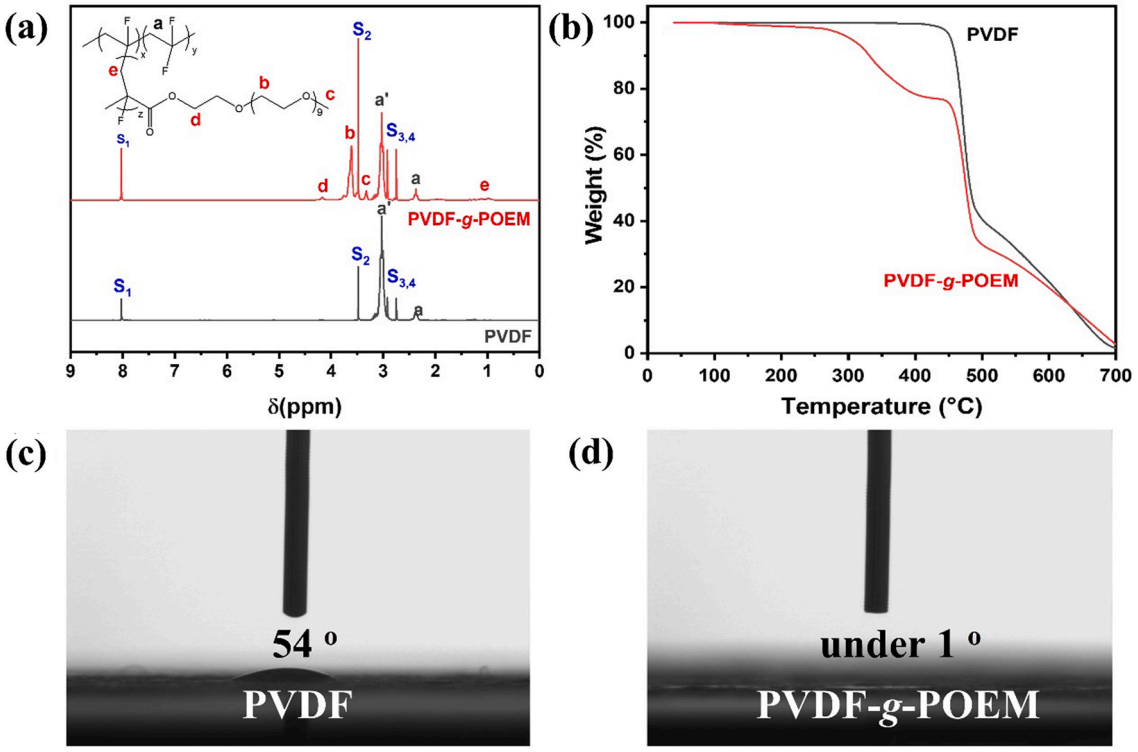

Fig. 3. (a) ^{1}H NMR spectra, (b) TGA of hydrophobic PVDF and amphiphilic PVDF-*g*-POEM double comb copolymer. Images of the water contact angle on the conducting side of the FTO substrate with (c) hydrophobic PVDF and (d) amphiphilic PVDF-*g*-POEM double comb copolymer coating, respectively.

stabilities of the amphiphilic PVDF-*g*-POEM double comb copolymer were also investigated by TGA as shown in Fig. 3**b**. The hydrophobic PVDF showed excellent thermal stability up to 450 °C, above which it started to decompose to around 40 wt%. Meanwhile, the significant weight losses for amphiphilic PVDF-*g*-POEM double comb copolymer were observed around 300–425 °C, attributable to the thermal degradation of POEM part of amphiphilic PVDF-*g*-POEM double comb copolymer. The TGA data represent that the amphiphilic PVDF-*g*-POEM double comb copolymer is thermally stable up to around 300 °C. The relative wettability of the hydrophobic PVDF, amphiphilic PVDF-*g*-POEM double comb copolymer were obtained using water contact angle measurements as shown in Fig. 3**c,d**. The contact angle measurements were conducted using the polymer solution spin-coated onto the conductive side of fluorine-doped tin oxide substrate. A water droplet placed on a hydrophobic PVDF showed a high contact angle (54°), which changes very little over time until the drop finally evaporates. PVDF exhibited a high contact angle (54°) that hardly changed over time until the droplets finally evaporated. It should be noted that our suggested membrane based on PVDF or PVDF-*g*-POEM is a highly porous state resulted in shown low contact angle value compare to the dense polymer-based membrane. However, a water droplet placed on an amphiphilic PVDF-*g*-POEM double comb copolymer showed a contact angle that decreases to under 1° over time. These results suggesting that the existence of hydrophilic POEM of amphiphilic PVDF-*g*-POEM double comb copolymer further increased wettability.

3.2. Morphology and filtration efficiency of the nanofibrous air filter membrane

To demonstrate the improved chemical and physical adsorption properties of nanofibrous air filter membrane based on amphiphilic PVDF-*g*-POEM double comb copolymer compared to those of hydrophobic PVDF, the two types of polymer solutions were electrospun to nanofibers under a high electric field and characterized, respectively. The FT-IR spectra of nanofibrous air filter membrane based on hydrophobic PVDF and amphiphilic PVDF-*g*-POEM double comb copolymer are shown in **Figure S1**. In the spectrum obtained after the POEM was introduced to PVDF, new absorption bands appear at 840 cm^{-1}, which correspond to the β phases of amphiphilic PVDF-*g*-POEM double comb copolymers. These results again confirmed that the hydrophilic POEM side chain played a significant role as a molecular directing agent to control the phase of nanofibrous air filter membrane based on amphiphilic PVDF-*g*-POEM double comb copolymer. The FE-SEM images and diameter distribution in Fig. 4 show the morphologies of the two electrospun nanofibrous air filter membranes, which clearly points out the effective impact of the amphiphilic PVDF-*g*-POEM double comb copolymer in terms of the ultrathin diameter of the resultant nanofibers (77.53 nm) compared to that of the hydrophobic PVDF (556.8 nm). This possibly occurs owing to the enhanced electronegativity of the additional oxygen atoms in the POEM chains and improved electrostatic attraction of the fluorine atom in hydrophobic PVDF, which effectively promotes the generation of the β phase and simultaneously triggers strong coulombic interactions; these effects mitigate the surface tension of the amphiphilic PVDF-*g*-POEM double comb copolymer solution compared to that of hydrophobic PVDF. [40] It is noteworthy that the addition of hydrophilic components is known to enable a reduction in surface energy, resulting in an improvement in the stretchability of the copolymer jet and the production of thin nanofibers. [41]

The filtration performance of nanofibrous air filter membrane based on hydrophobic PVDF and amphiphilic PVDF-*g*-POEM double comb copolymer is shown in Fig. 5. Fig. 5**a** shows a clear improvement in the filtration performance of nanofibrous air filter membrane based on amphiphilic PVDF-*g*-POEM double comb copolymer compared to that of hydrophobic PVDF, particularly at the low pressure drop region (less than5mmH_2O). Specifically, in Fig. 5**b**, the nanofibrous air filter membranes based on hydrophobic PVDF show low filtration efficiency of less

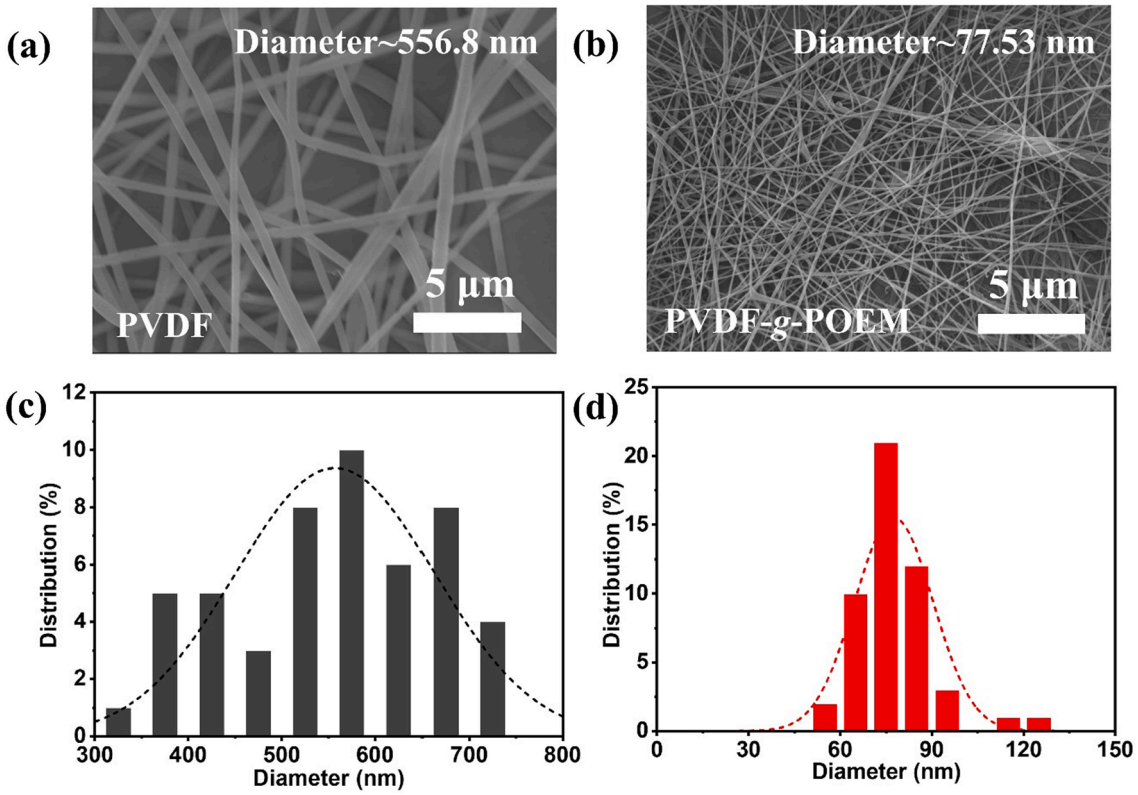

Fig. 4. FE-SEM images and diameter distribution of nanofibrous air filter membrane based on (a,c) hydrophobic PVDF and (b,d) amphiphilic PVDF-*g*-POEM double comb copolymer.

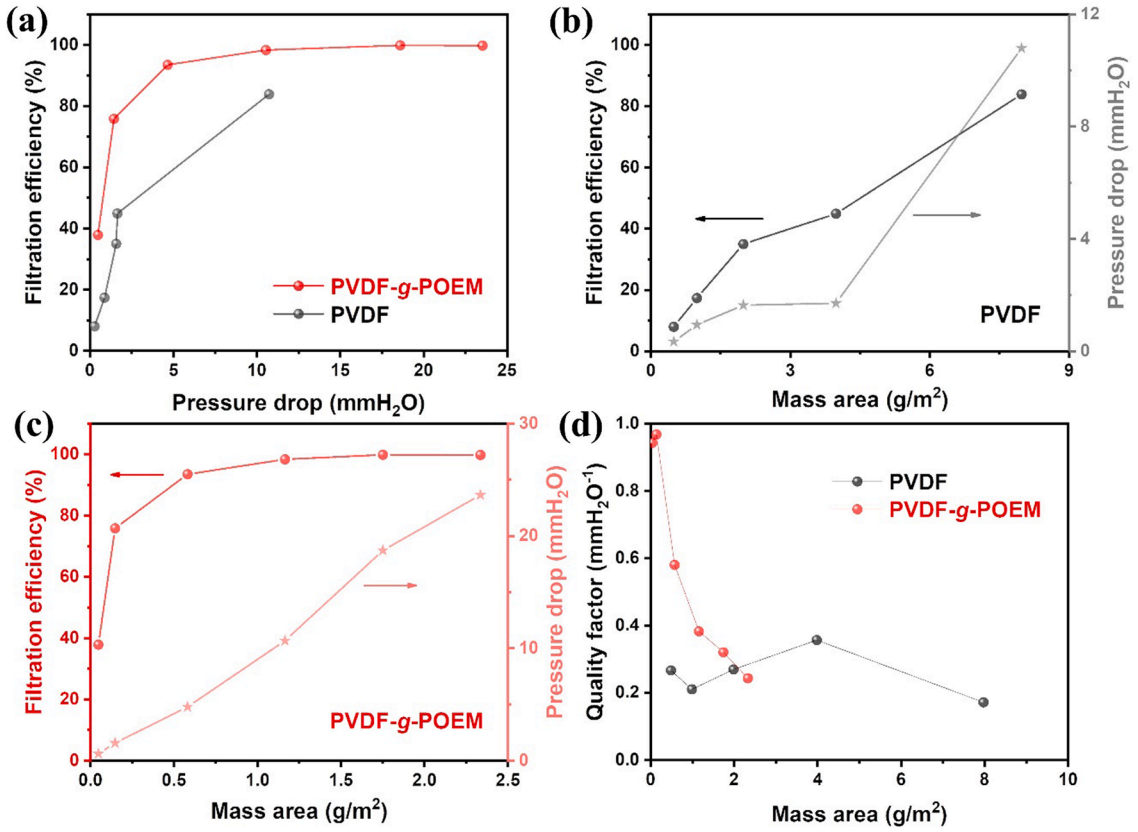

Fig. 5. (a) Filtration efficiency of nanofibrous air filter membrane based on hydrophobic PVDF and amphiphilic PVDF-*g*-POEM double comb copolymer as a function of pressure drop, (b) Filtration efficiency and pressure drop of hydrophobic PVDF based nanofibrous air filter membrane as a function of basis weights, (c) amphiphilic PVDF-*g*-POEM double comb copolymer based nanofibrous air filter membrane as a function of basis weights and (d) quality factor of nanofibrous air filter membrane based on hydrophobic PVDF and amphiphilic PVDF-*g*-POEM double comb copolymer as a function of mass area.

than 50% even though the mass area is increased up to 4 g/m^2. It reaches filtration efficiency of 83% at loaded mass area around 8 g/m^2 with the significant escalation of pressure drop to more than 10 mmH$_2$O. Meanwhile, as shown in Fig. 5**c**, the nanofibrous air filter membrane based on amphiphilic PVDF-*g*-POEM double comb copolymer exhibits the high filtration efficiency of 75.6% and a relatively low pressure drop of 1.46 mmH$_2$O at significantly low mass area of 0.15 g/m^2 which result the highest quality factor of 0.967 mmH$_2$O^{-1}. The nanofibrous air filter membrane based on amphiphilic PVDF-*g*-POEM double comb copolymer shows the filtration efficiency higher than 93% with a sufficient quality factor of 0.59 mmH$_2$O^{-1}, as shown in **Figure S2**. The superior air filtration performance of the amphiphilic PVDF-*g*-POEM nanofibrous membranes against the pristine PVDF nanofibrous membranes are clearly depicted in Fig. 5**d** *via* the quality factor as a function of mass area. However, as a rule of thumb, the higher deposited mass area filter will result in a huge value of area resistance or pressure drop and thereby degrading the quality factor of the entire filter. For a more reasonable comparison, the nanofibrous air filter membrane based on amphiphilic PVDF-*g*-POEM double comb copolymer was made at an ultra-low mass area of 0.05 g/m^2 with single-nozzle electrospinning to intentionally degrade the filtration efficiency of the modified polymer. **Figure S2** apparently shows the quality factor difference between nanofibrous air filter membrane based on amphiphilic PVDF-*g*-POEM double comb copolymer and the nanofibrous air filter membrane based on hydrophobic PVDF at low filtration efficiency level, specifically the nanofibrous air filter membrane based on amphiphilic PVDF-*g*-POEM double comb copolymer exhibited the filtration efficiency of 37.56 % relevant to the quality factor of 0.942 mmH$_2$O^{-1} which is much higher than that of the poor quality factor of the nanofibrous air filter membrane based on hydrophobic PVDF (0.266 mmH$_2$O^{-1}) shown in the same figure due to large observed pressure drop. For better comprehension on the reliability of long-term usage, the nanofibrous air filter membranes based on amphiphilic PVDF-*g*-POEM double comb copolymer and hydrophobic PVDF were completely immersed in isopropanol (IPA) solvent for various periods of time, and the obtained results are shown in **Figure S3**. **Figure S3a** displays the superior filtration performance durability of the amphiphilic PVDF-*g*-POEM nanofibrous membrane against polypropylene MB filter membrane. The filtration efficiency of polypropylene MB filter membrane dramatically degrades after 1 h immersed in IPA bath. Meanwhile, the amphiphilic PVDF-*g*-POEM nanofibrous membrane shows the filtration efficiency retention of 91.92 % after 10 h exposure in IPA. Moreover, compared to hydrophobic PVDF nanofibrous membrane, the amphiphilic PVDF-*g*-POEM filter also possesses a greater filtration performance retention shown in **Figure S3b.** Although there could be some residual electrostatic charge for PVDF and PVDF-*g*-POEM, the significantly enhanced filtration performance retention of PVDF-*g*-POEM after IPA exposure supports the existence of chemical functionality in addition to slip effect with thinner filter diameter, which can contribute to improving the shortcoming on particles loading of nanofiber-based filter due to two dimensional nature. In general, the enhancement in air filtration performance of the nanofibrous air filter membrane based on amphiphilic PVDF-*g*-POEM double comb copolymer can be possibly attributed to the dual effects of the synthesized copolymer. The facile interactions among the ultrathin amphiphilic PVDF-*g*-POEM double comb copolymer-based nanofibers, which are closer in size (77.53 nm) to the mean free path of air molecules (65.3 nm), generate a slip effect region for air molecules to bypass the nanofibers; this leads to a pressure drop reduction and a simultaneous improvement in air filtration efficiency, as shown in Scheme 3. In addition, although the nanofibrous air filter membrane based on

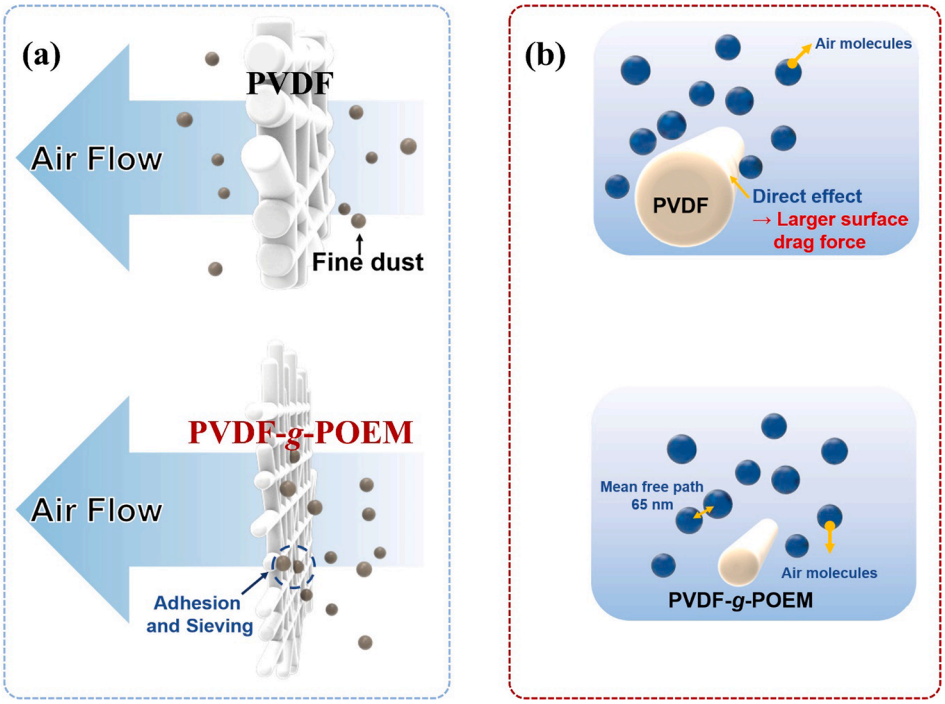

Scheme 3. (a) Schematic diagram of filtration, (b) air-flow regime of nanofibrous air filter membrane based on hydrophobic PVDF and amphiphilic PVDF-*g*-POEM double comb copolymer.

amphiphilic PVDF-*g*-POEM double comb copolymer exhibited a slightly higher pressure drop, the higher electronegativity of PVDF-*g*-POEM enables an enhancement in the quality factor and filtration efficiency. Notably, the amphiphilic PVDF-*g*-POEM double comb copolymer with buffer interactions between the hydrophobic main chain of PVDF and the hydrophilic side chain of POEM enables the capture of both negative and positive charges of particles with high chemical affinity.

4. Conclusions

The nanofibrous air filter membrane based on amphiphilic PVDF-*g*-POEM double comb copolymer were successfully fabricated in this study *via* ATRP and electrospinning, which effectively reduced the diameter of the fibers to the slip flow region with lower air resistance. Fine dust was readily captured by enhanced chemical and physical adsorption properties of nanofibrous air filter membrane due to the amphiphilic characteristics of PVDF-*g*-POEM double comb copolymer, which resulted in enhanced air filtration efficiency and lower air resistance compared to those of the hydrophobic PVDF. This synthesis strategy for nanofibrous air filter membrane based on amphiphilic PVDF-*g*-POEM double comb copolymer may be applied to the development of efficient air filters to sieve $PM_{0.3}$ pollutants.

CRediT authorship contribution statement

Juyoung Moon: Methodology, Validation. **Tan Tan Bui:** Methodology, Validation. **Soyoung Jang:** Data curation. **Seungyoung Ji:** Data curation. **Jung Tae Park:** Supervision. **Myung-Gil Kim:** Supervision.

Declaration of Competing Interest

The authors declare that they have no known competing financial interests or personal relationships that could have appeared to influence the work reported in this paper.

Acknowledgements

This work was supported by the National Research Foundation of Korea (NRF) grant funded by the Korea government (MSIP) (NRF-2019R1C1C1010283, NRF-2020R1A2C4001617). This work was supported by the Technology Innovation Program (20004627) funded by the Ministry of Trade, Industry & Energy (MOTIE, Korea).

Appendix A. Supplementary material

Supplementary data to this article can be found online at https://doi.org/10.1016/j.seppur.2021.119625.

References

[1] Y.u. Wang, H. Tian, L.i. Zhang, M. Zhang, D. Guo, W. Wu, X. Zhang, G.L. Kan, L. Jia, D.a. Huo, B. Liu, X. Wang, Y. Sun, Q. Wang, P. Yang, C.R. MacIntyre, Reduction of secondary transmission of SARS-CoV-2 in households by face mask use, disinfection and social distancing: a cohort study in Beijing, China, BMJ Glob. Health 5 (5) (2020) e002794, https://doi.org/10.1136/bmjgh-2020-002794.
[2] J. Howard, A. Huang, Z. Li, Z. Tufekci, V. Zdimal, H.M. van der Westhuizen, A. von Delft, A. Price, L. Fridman, L.H. Tang, An evidence review of face masks against COVID-19, Proc. Natl. Acad. Sci. U. S. A. 118 (2021) e2014564118.
[3] K.-H. Kim, E. Kabir, S. Kabir, A review on the human health impact of airborne particulate matter, Environ. Int. 74 (2015) 136–143.
[4] J.D. Sacks, L.W. Stanek, T.J. Luben, D.O. Johns, B.J. Buckley, J.S. Brown, M. Ross, Particulate matter–induced health effects: who is susceptible? Environ. Health Perspect. 119 (4) (2011) 446–454.
[5] L.W. Stanek, J.D. Sacks, S.J. Dutton, J.J.B. Dubois, Attributing health effects to apportioned components and sources of particulate matter: an evaluation of collective results, Atmos. Environ. 45 (2011) 5655–5663.
[6] C.J. Lee, R.V. Martin, D.K. Henze, M. Brauer, A. Cohen, A.V. Donkelaar, Donkelaar, Response of global particulate-matter-related mortality to changes in local precursor emissions, Environ. Sci. Technol. 49 (7) (2015) 4335–4344.
[7] A. Podgórski, A. Bałazy, L. Gradoń, Application of nanofibers to improve the filtration efficiency of the most penetrating aerosol particles in fibrous filters, Chem. Eng. Sci. 61 (20) (2006) 6804–6815.
[8] K.W. Lee, B.Y.H. Liu, On the minimum efficiency and the most penetrating particle size for fibrous filters, J. Air Pollut. Control. Assoc. 30 (4) (1980) 377–381.
[9] N.J. Rowan, R.A. Moral, Disposable face masks and reusable face coverings as non-pharmaceutical interventions (NPIs) to prevent transmission of SARS-CoV-2 variants that cause Coronavirus disease (COVID-19): role of new sustainable NPI design innovations and predictive mathematical modelling, Sci. Total Environ. 772 (2021) 145530.

[10] K.P. Lee, J. Yip, C.W. Kan, J.C. Chiou, K.F. Yung, Reusable face masks as alternative for disposable medical masks: factors that affect their wear-comfort, Int. J. Environ. Res. Public Health 17 (2020) 6623.
[11] S. Ullah, A. Ullah, J. Lee, Y. Jeong, M. Hashmi, C. Zhu, K.I. Joo, H.J. Cha, I.S. Kim, Reusability comparison of melt-blown vs nanofiber face mask filters for use in the coronavirus pandemic, ACS Appl. Nano Mater. 3 (2020) 7231–7241.
[12] K. O'Dowd, K.M. Nair, P. Forouzandeh, S. Mathew, J. Grant, R. Moran, J. Bartlett, J. Bird, S.C. Pillai, Face masks and respirators in the fight against the COVID-19 pandemic: a review of current materials, advances and future perspectives, Materials 13 (2020) 3363.
[13] R.K. Campos, J. Jin, G.H. Rafael, M. Zhao, L. Liao, G. Simmons, S. Chu, S. C. Weaver, W. Chiu, Y.i. Cui, Decontamination of SARS-CoV-2 and other RNA viruses from N95 level meltblown polypropylene fabric using heat under different humidities, ACS nano 14 (10) (2020) 14017–14025.
[14] Y. Lee, L.C. Wadsworth, Structure and filtration properties of melt blown polypropylene webs, Polym. Eng. Sci. 30 (22) (1990) 1413–1419.
[15] H.-J. Choi, E.-S. Park, J.-U. Kim, S.H. Kim, M.-H. Lee, Experimental study on charge decay of electret filter due to organic solvent exposure, Aerosol Sci. and Technol. 49 (10) (2015) 977–983.
[16] Y. Xiao, Y. Wang, W. Zhu, J. Yao, C. Sun, J. Militky, M. Venkataraman, G. Zhu, Development of tree-like nanofibrous air filter with durable antibacterial property, Sep. Purif. Technol. 259 (2021) 118135.
[17] Q. Qi, W. Wang, Y. Wang, D. Yu, Robust light-driven interfacial water evaporator by electrospinning SiO_2/MWCNTs-COOH/PAN photothermal fiber membrane, Sep. Purif. Technol. 239 (2020) 116595.
[18] Y. Yang, Y. Li, L. Cao, Y. Wang, L. Li, W. Li, Electrospun PVDF-SiO_2 nanofibrous membranes with enhanced surface roughness for oil-water coalescence separation, Sep. Purif. Technol. 269 (2021) 118726.
[19] X. Zhao, S. Wang, X. Yin, J. Yu, B. Ding, Slip-effect functional air filter for efficient purification of PM 2.5, Sci. Rep. 6 (2016) 1–11.
[20] H.-J. Choi, M. Kumita, T. Seto, Y. Inui, L.i. Bao, T. Fujimoto, Y. Otani, Effect of slip flow on pressure drop of nanofiber filters, J. Aerosol. Sci. 114 (2017) 244–249.
[21] L.i. Bao, K. Seki, H. Niinuma, Y. Otani, R. Balgis, T. Ogi, L. Gradon, K. Okuyama, Verification of slip flow in nanofiber filter media through pressure drop measurement at low-pressure conditions, Sep. Purif. Technol. 159 (2016) 100–107.
[22] T. Xia, Y.e. Bian, L.i. Zhang, C. Chen, Relationship between pressure drop and face velocity for electrospun nanofiber filters, Energy Build. 158 (2018) 987–999.
[23] K. Matyjaszewski, J. Xia, Atom transfer radical polymerization, Chem. Rev. 101 (9) (2001) 2921–2990.
[24] C.-Y. Hsu, R.-J. Liu, C.-H. Hsu, P.-L. Kuo, High thermal and electrochemical stability of PVDF-*graft*-PAN copolymer hybrid PEO membrane for safety reinforced lithium-ion battery, RSC Adv. 6 (22) (2016) 18082–18088.
[25] K.-M. Kim, S. Woo, J.u. Lee, H. Park, J. Park, B. Min, Improved permeate flux of PVDF ultrafiltration membrane containing PVDF-*g*-PHEA synthesized *via* ATRP, Appl. Sci. 5 (4) (2015) 1992–2008.
[26] J.-Q. Meng, C.-L. Chen, L.-P. Huang, Q.-Y. Du, Y.-F. Zhang, Surface modification of PVDF membrane via AGET ATRP directly from the membrane surface, Appl. Surf. Sci. 257 (14) (2011) 6282–6290.
[27] M. Tao, F.u. Liu, L. Xue, Hydrophilic poly (vinylidene fluoride)(PVDF) membrane by in situ polymerisation of 2-hydroxyethyl methacrylate (HEMA) and micro-phase separation, J. Mater. Chem 22 (18) (2012) 9131, https://doi.org/10.1039/c2jm30695f.
[28] H. Liu, S. Zhang, L. Liu, J. Yu, B. Ding, High-Performance PM0. 3 Air Filters Using Self-Polarized Electret Nanofiber/Nets, Adv. Funct. Mater. 30 (2020) 1909554.
[29] Y. Xiao, E. Wen, N. Sakib, Z. Yue, Y. Wang, S.i. Cheng, J. Militky, M. Venkataraman, G. Zhu, Performance of electrospun polyvinylidene fluoride nanofibrous membrane in air filtration, Autex Res. J. 20 (4) (2020) 552–559.
[30] J.Y. Zheng, M.F. Zhuang, Z.J. Yu, G.F. Zheng, Y. Zhao, H. Wang, D.-H. Sun, The effect of surfactants on the diameter and morphology of electrospun ultrafine nanofiber, J. Nanomater. 2014 (2014) 689298.
[31] Z. Li, W. Kang, H. Zhao, M. Hu, J. Ju, N. Deng, B. Cheng, Fabrication of a polyvinylidene fluoride tree-like nanofiber web for ultra high performance air filtration, RSC Adv. 6 (94) (2016) 91243–91249.
[32] G.H. Choi, S.M. Lim, J. Moon, J.M. Lim, U.C. Baek, J.T. Park, Synthesis of Ag_2O decorated hierarchical TiO_2 templated by double comb copolymers for efficient solar water splitting, Chem. Commun. 55 (2019) 11013.
[33] J.Y. Lee, G.H. Choi, J. Moon, W.S. Chi, J.T. Park, 1D Co_4S_3 nanoneedle array with mesoporous carbon derived from double comb copolymer as an efficient solar conversion catalyst, Appl. Surf. Sci. 535 (2021) 147637.
[34] G.H. Choi, K. Kang, G.S. Hwang, Y.-J. Kim, Y.-K. Kim, Y.-R. Kim, J.T. Park, H. Jang, Surface-controlled galvanic replacement for the development of Pt-Ag nanoplates with concave surface substructures, Chem. Eng. J. 417 (2021) 128026.
[35] J.T. Park, W.S. Chi, H. Jeon, J.H. Kim, Improved electron transfer and plasmonic effect in dye-sensitized solar cells with bi-functional Nb-doped TiO_2/Ag ternary nanostructures, Nanoscale 6 (2014) 2718.
[36] R. Gregorio, Jr., M. Cestari, Effect of crystallization temperature on the crystalline phase content and morphology of poly (vinylidene fluoride), J. Polym. Sci. B. Polym. Phys. 32 (5) (1994) 859–870.
[37] C. Marega, A. Marigo, Influence of annealing and chain defects on the melting behaviour of poly(vinylidene fluoride), Eur. Polym. J. 39 (8) (2003) 1713–1720.
[38] D.R. Dillon, K.K. Tenneti, C.Y. Li, F.K. Ko, I. Sics, B.S. Hsiao, On the structure and morphology of polyvinylidene fluoride-nanoclay nanocomposites, Polymer 47 (5) (2006) 1678–1688.
[39] M.R. Moghareh Abed, S.C. Kumbharkar, A.M. Groth, K. Li, Economical production of PVDF-*g*-POEM for use as a blend in preparation of PVDF based hydrophilic hollow fibre membranes, Sep. Purif. Technol. 106 (2013) 47–55.
[40] K.-Y. Law, Definitions for hydrophilicity, hydrophobicity, and superhydrophobicity: getting the basics right, J. Phys. Chem. Lett. 5 (4) (2014) 686–688.
[41] T. Zhang, R.E. Marchant, Novel polysaccharide surfactants: The effect of hydrophobic and hydrophilic chain length on surface active properties, J. Colloid Interface Sci. 177 (1996) 419–426.